HAL
open science

An object oriented approach for quantitative assessment of building damage in urban areas using very high resolution images

Anne-Lise Chesnel, Renaud Binet, Lucien Wald

An object oriented approach for quantitative assessment of building damage in urban areas using very high resolution images

Anne-Lise Chesnel and Renaud Binet
Commissariat à l'Energie Atomique
Département Analyse et Surveillance de l'Environnement
91680 Bruyères-le-Châtel, France
Email: anne-lise.chesnel@cea.fr, renaud.binet@cea.fr

Lucien Wald
Ecole des Mines de Paris
Centre Energétique et Procédés
06904 Sophia-Antipolis, France
Email: lucien.wald@ensmp.fr

Abstract—**Very High Resolution images are particularly well adapted to damage assessment in urban area because on one hand it allows an analysis focused on the buildings solely through an object-oriented analysis, and on the other hand it permits a quantitative evaluation of this damage assessment using a visually established *ground truth*. We proposed in this paper a method of damage assessment that uses these two benefits. First an original object oriented approach to register the images is presented. Then a simple and fast damage assessment method based on correlation is proposed and tested on several test-cases. Each buildings of a test-area is classified using Support Vector Machines. The performances of the method in each case is evaluated thanks to a manually constructed reference database that uses the European Macroseismic Scale. Our method shows good results, with up to 75% of buildings well classified among four different EMS damage grades.**

I. INTRODUCTION

Natural disasters impact an increasing number of persons. A large part of the human and economical losses are due to the destruction of constructions, where people live and work. Damage assessment in an urban context is of interest because the concentration of buildings makes these implications more important. Very High Resolution (VHR) images, i.e. with spatial resolution better than 1m, offer a strong potential to achieve this evaluation because it allows identification of changes on buildings. However, this assessment is time-consuming because of the number of objects to be analysed. An automated data processing could help [1].

Our present work focuses on the roof of buildings to assess damage. The perception of roofs is less affected by changes in viewing angle than other parts of a building. Moreover, roofs are visible by means of remote sensing and it is expected that they are less concerned with other changes. We estimate that, most of the time, damage corresponding to grades 4 and 5 on the European Macroseismic Scale (EMS) [2] can be detected in VHR images by analysing roofs, because the roofs are often affected by heavy structural damage. However a collapse of a soft storey (e.g. ground floor) is for example undetectable on the roof itself. Grade 3 can be detected at

times but in a less reliable way [3], [4]. Damage inside the buildings and cracks on the walls cannot be detected, notably regarding for the spatial resolution of the actual sensors; buildings with a EMS damage grade lower that 3 will be considered as intact (grade 0) in our work. Thus, 4 distinct damage grades will be considered in this study.

Methods based on VHR images face new challenges [5]–[8]. The natural changes are more numerous as the resolution increases, leading to new difficulties: shadows changes, apparitions and disappearances of objects due to the human activity (e.g. cars, refugees tents). In addition the relative influence of errors in registration of building roofs increases [6]. Pixel-based methods are more sensitive to these problems and show higher false-alarm rates [6], [9]. They may not allow to distinguish damage from other changes. Recently, more attention is given to region-based methods with VHR images, reducing a part of the problems quoted above. We have chosen such an approach. However, the task of building extraction is not dealt within this work, since it represents a problem in itself [10]–[15]. Instead, we suppose that we are in the ideal situation where we have an a priori knowledge of the buildings footprint in the reference image.

Our approach is divided in four steps. Firstly, the footprints of the roofs of buildings are segmented in the reference image. The roofs in the two images, the reference and crisis images, are then registered by a correlation method. In a third step, pixel-based tools for change detection are used to assess the damage on the roofs alone. The buildings are classified in the fourth step. A reference database has been built independently and is used as a reference for registration of roofs (second step), training for classification (fourth step) and assessment of the performance of the approach.

This approach is applied to several cases: the Bam (Iran) earthquake of December 26, 2003; the Boumerdes (Algeria) earthquake of May 21, 2003; the Muzzafarabad (Pakistan) earthquake of October 8, 2005; and the Ryongchon (North Korea) train explosion of April 22, 2004. Two VHR sensors are used: QuickBird and Ikonos, with respectively

a spatial resolution of 60cm and 1m. The evaluation of the performance of our method is made by comparison to the reference database. The effectiveness of the method is quantitatively evaluated as a function of the test case, of the spatial resolution of these images, and of the damage degree. Thus the application domain and the limits of the registration method are investigated.

II. IMAGES AND REFERENCE DATABASES

The images used in this study are panchromatic VHR images from QuickBird [16] and Ikonos [17] sensors (table I). These sensors respectively enable spatial resolution equal to 60cm and 1m at nadir. The images of each cases of study have different acquisition parameters (table I). The elevation and azimuth of the sun are also different due to the season change. Different combinations of images from the two sensors acquired before and after each events are used (table II). In the case of a multi-sensor images (e.g. QuickBird/Ikonos), the image with higher resolution is downsampled to the resolution of the other. For that purpose, an apodised sinc, with a window size equal to 21 pixels is used. The image before the event is the reference image, and the image after is the crisis image.

The registration method is applied to several cases of urban disaster: the Bam (Iran) earthquake of December 26, 2003; the Boumerdes (Algeria) earthquake of May 21, 2003; the Muzzafarabad (Pakistan) earthquake of October 8, 2005; and the Ryongchon (North Korea) train explosion of April 22, 2004. In each test case, the buildings and the damage on them differ by some aspects. We investigate the robustness of our registration method with these varied cases.

We have constructed one database per case to serve as a reference to assess the performances of our approach. It contains the footprints of the roofs of the buildings prior to the disaster. The footprints were manually extracted from the reference images. For example, in the case of the Bam earthquake, 2168 buildings are contained in this database, and they are located in the eastern part of the town. An extract of the Bam QuickBird reference image on which the footprints of the buildings have been overlaid is presented in figure 1. The other databases contain respectively 610 buildings in Boumerdes, 725 buildings in Ryongchon and 937 buildings in Muzzafarabad.

III. REGISTRATION

Standard methods for image registration do not allow registration of buildings of unknown heights when the off-nadir viewing angles differ from one image to another [6], [18]. Thus the footprint of the buildings roofs have to be registered prior to the analysis of changes, by computing individually the offset for each building. First, the two images are roughly registered; the ground registration error is estimated to be at most three pixels. Then the registration of the buildings roof is conducted with a subpixel accuracy. The buildings in the crisis
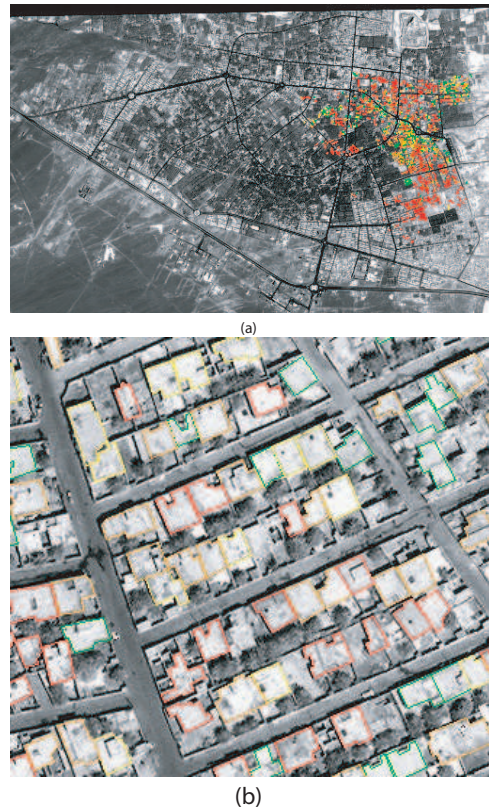

Fig. 1. QuickBird reference image (before the earthquake) of Bam. The buildings footprint of the corresponding reference database is overlaid. (a) : entire scene; (b) : image extract. Colour legend of the database: Green = damage grade 0; Yellow = damage grade 3; Orange = damage grade 4; Red = damage grade 5. Images: copyright DigitalGlobe 2003, 2004.

TABLE I
IMAGES USED. QB=QUICKBIRD AND IK=IKONOS

Area	Sensor	Date	Sat. elevation angle above the horizon	Sat. azimuth (clockwise due North)
Bam (Iran)	QB	2003-03-30	78.8^o	191.9^o
	QB	2004-01-03	63.3^o	233.8^o
	IK	2004-01-04	62.9^o	132.1^o
Boumerdes (Algeria)	QB	2002-04-22	78.6^o	352.8^o
	QB	2003-05-23	64.2^o	276.5^o
Muzzafarabad (Pakistan)	QB	2004-08-13	79.4^o	151.4^o
	QB	2005-10-22	64.8^o	118.6^o
	IK	2002-09-15	71.7^o	227.8^o
	IK	2005-10-09	79.7^o	306.7^o
Ryongchon (North Korea)	QB	2003-05-13	59.9^o	274.1^o
	QB	2004-04-27	72.6^o	282.8^o

TABLE II
CASE OF STUDY. QB=QUICKBIRD AND IK=IKONOS

| before/after | Events | | | |
	Bam[a]	Boumerdes[a]	Muzzafarabad[a]	Ryongchon[b]
QB/QB	x	x	x	x
IK/IK			x	
QB/IK	x			
IK/QB				
QB$_{1m}$/QB$_{1m}$	x	x		x

[a]Earthquake
[b]Explosion

image do not need to be segmented to extract the buildings; the registration process uses solely the footprint of the buildings of the reference database.

A. Image registration

The QuickBird images are orthorectified by the mean of the SRTM Digital Terrain Model (3 arcsec) to compensate for the ground elevation, the Rational Polynomial Coefficients (RPC) provided with the QuickBird data to model the sensor and a set of four ground control points in order to compensate the pointing error. The Ikonos images were already orthorectified. The crisis image is registered to the reference image using a cubic convolution interpolation method. For both type of images, the remaining registration error of the ground is due to the imprecision of the DTM and/or RPC modelling error. It can be considered as locally constant. It is constant in the image for an area with smooth relief; steep relief can make it more varying if not accurately corrected. In addition, the images having different viewing angles, roofs of buildings are not registered precisely; considering each pair of images, as the offset is proportional to the height of the building, it can differ for each roof. We have devised a method for assessing and correcting those offsets for each roof.

B. Roof registration

Our registration method estimates the maximum a posteriori of a similarity measurement. This measurement is the correlation (equation 1) computed on the group of pixels held in the roof footprints on both images. In the reference image, the footprint is specified by the manual segmentation. This footprint is translated in the crisis image by a quantity $\vec{o}$ estimated by the algorithm of roofs registration (equation 1). Let I_1 and I_2 be respectively the reference and the crisis images. Let c and l be respectively the column and the line coordinates, and k_c and k_l be respectively the shift value of the footprint of the roof in the crisis image along the columns and along the lines.

$$R_i(c,l) = I_i(c,l).H(c,l) - \frac{\sum\limits_{c,l} I_i(c,l).H(c,l)}{\sum\limits_{c,l} H(c,l)},$$

$$\text{for } i = \{1, 2\},$$

$$\vec{o} = \arg\max_{k_c,k_l}\left\{\frac{\sum\limits_{c,l} R_1(c,l).R_2(c+k_c,l+k_l)}{\sqrt{\sum\limits_{c,l} R_1^2(c,l)}.\sqrt{\sum\limits_{c,l} R_2^2(c+k_c,l+k_l)}}\right\},$$

$$\text{for } \{c,l | H(c,l) = 1\} \quad (1)$$

$$\text{where } H(c,l) = \begin{cases} 1 & \text{if } I_1(c,l) \in \text{roof footprint} \\ 0 & otherwise \end{cases}$$
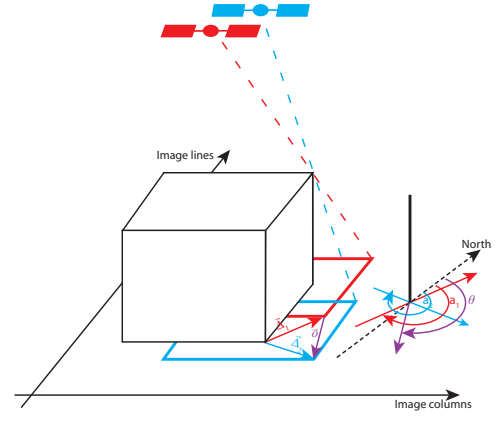

Fig. 2. Illustration of the direction θ, along which the roof projection of the buildings moves between the images, as a function of the angles of acquisition of each image.

The function $H(c,l)$ may be defined by the means of the segmentation of buildings footprint as discussed earlier. In our case, its values are assigned by the means of the reference database of buildings. The position (k_c^*, k_l^*) of the maximum correlation yields the offset $\vec{o}$. Equation (1) is applied to a limited search area. Defining this search area is the first challenge. If it is too small, one may not find the true maximum correlation and underestimate the offset. Conversely if it is too large, it is likely that the correlation peak does not correspond to the right result, especially in urban area where edge features are numerous and have often the same orientation. The second challenge is that when considering a damaged building, the correlation has no sense because there is no similarity at all between the roof in the reference image and the corresponding place in the crisis image. One should find a way to retrieve the correct location of the building remains. In the following we propose a method to find out an adapted search area.

The offset $\vec{o}$ can be written as the sum of a ground offset $\vec{o_g}$ due to the ground misregistration and a height offset $\vec{o_h}$ due to the unknown height of the building: $\vec{o} = \vec{o_g} + \vec{o_h}$. Let $\vec{o_\perp}$ be such that $\vec{o_g} \wedge \vec{o_\perp} = \vec{0}$.

The ground offset $\vec{o_g}$ has no expectable orientation. On the contrary, the height offset $\vec{o_h}$ is solely dependent on the viewing angles for both images (direction) and on the height of the building (amplitude). Except for pancaked buildings (soft story collapse), this offset is observed in an *epipolar-like* direction θ given by the equation (2). Figure 2 illustrates how θ is defined as a function of the viewing angles of the two images.

$$\theta = \arctan\left\{\frac{\tan e_1 \sin a_2 - \tan e_2 \sin a_2}{\tan e_1 \cos a_2 - \tan e_2 \cos a_2}\right\} \quad (2)$$

where a_1, e_1, a_2, e_2 are respectively the satellite azimuth and elevation angle above horizon of the reference and crisis images (table I).

The height offset is due to the height of the constructions,

so its amplitude differs for each building. On the contrary, we will suppose that the ground offset does not vary much. These differences are exploited to define the search area. Note that a 2D search is necessary due to the unpredictability of the ground offset, reducing the relevance of an epipolar image projection.

The search area is the same for all buildings. It is defined by the angle θ and by two search intervals defined along the axes $\vec{o_h}$ and $\vec{o_\perp}$ (figure 3). These search intervals are different along these directions. The roofs registration is divided in two steps. A first approximation of the search area (dotted rectangle in figure 3) is defined along the $\vec{o_\perp}$ axis by setting the search interval to $[-s, +s]$, where s is twice the expected registering error of the ground between the images (3 pixels in our case). Along the $\vec{o_h}$ axis, the interval is set to $[-s, s + s_h]$, where s_h is twice the roof offset associated to the highest building and is defined by:

$$s_h = 2h_{max}\sqrt{\left(\frac{\sin a_2}{\tan e_2} - \frac{\sin a_1}{\tan e_1}\right)^2 - \left(\frac{\cos a_2}{\tan e_2} - \frac{\cos a_1}{\tan e_1}\right)^2} \tag{3}$$

where h_{max} is the estimated maximum height of all the buildings.

An exhaustive computation over this whole first search area is conducted, and the correlation peak corresponds to the approximate roof offset of each building. A 2D histogram of the collection of offsets is built (figure 4). One may note, in the search area, points having very small values of occurrence which are outliers. It corresponds as a majority to damage buildings that do not exhibit correct offsets. In this case, they would corrupt the distribution of the offsets and should be filtered out. For that purpose, the histogram is fitted by a 2D Gaussian function, whose mean $(\mu_h, \mu_\perp)$ and standard deviation $(\sigma_h, \sigma_\perp)$ are estimated with a least square fit. The choice of a Gaussian function instead of another one is not very important since it serves only to compute a first approximation. The approximation of the roofs offset is then refined for each building. The offsets are computed on the new search area (plain rectangle in figure 3) centred on $(\mu_h, \mu_\perp)$ with intervals on each axis set to $[-8\sigma_h, +8\sigma_h]$ and $[-4\sigma_\perp, +4\sigma_\perp]$ (figures 3 and 4). Note that if there is no outlier, this computation would have no other action than centred the search area and refined the related tolerances in a better way.

Practically, the correlation values are computed by steps of 0.25 pixel in each orientation in the search region previously defined. A subpixel step is used for correlation, as the offset is not supposed to be a multiple of a pixel size. Thus it is necessary to compute a resampled version of the crisis image. For the first step of the registration, the bilinear interpolation is chosen as a good trade-off between efficiency and computational cost. We estimate that, except for the outlier values, the correlation peak is estimated with a 0.5 pixel accuracy. This is visible with the histogram in figure 4: offsets with an integer value seem more likely. This is
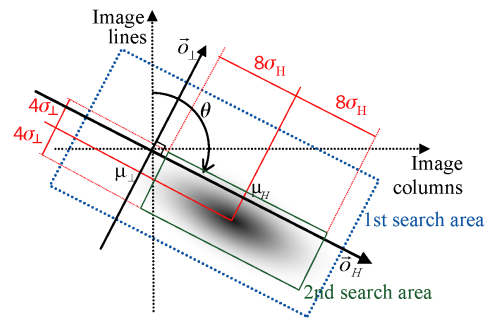

Fig. 3. Definition of the referential used for the registration computation. The ellipse depicts the 2D histogram of the offsets.
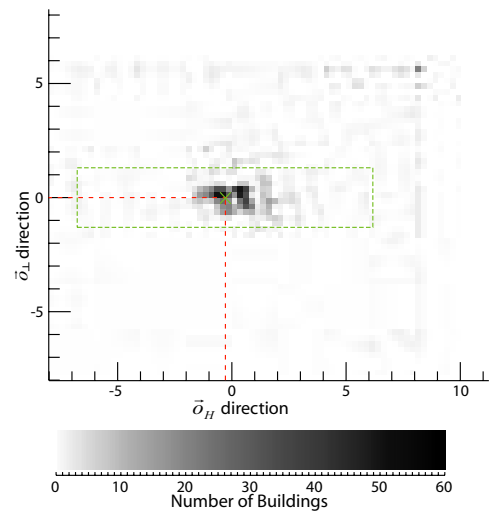

Fig. 4. A 2D histogram of the roof offsets computed in the first search area. The cross stands for the mean of the Gaussian fitted distribution; the dotted box will be the second search area obtained from the estimated distribution. The bilinear interpolation method used generates artefacts corresponding to integer values of offset in the $\vec{o_g}$ and $\vec{o_\perp}$ directions.

an artefact generated by the bilinear interpolation. The same computation can be done using a apodised sinc instead of the bilinear polynomial (figure 5): the artefact disappears but the computation for this step is very expensive (at least ten times more in our case). For the second step of the registration, an apodised sinc is used to resample the crisis image. The correlation peak value is estimated using a truncated-Newton optimization method to speed up the computation. The location of the peak, i.e. the roof offset, is thus estimated with a subpixel accuracy.

To improve the effectiveness of the correlation, the images are filtered by a Canny filter [19]. It emphasizes the important features (edges, elements on the roof) that characterize the buildings. This filtering especially allows a reduction of the radiometric changes in low frequencies and high frequencies (noise, aliasing) that are present in the images.
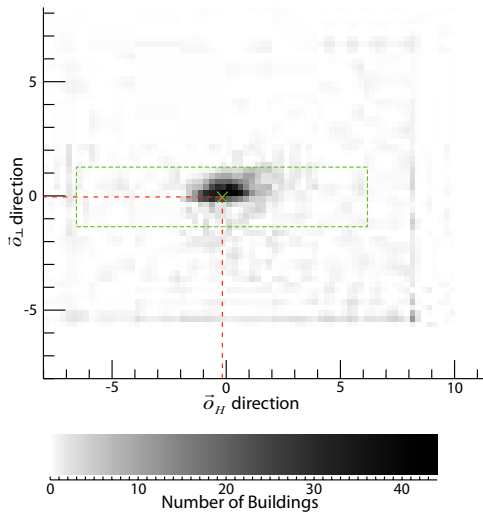
Fig. 5. A 2D histogram of the roof offsets computed in the first search area. The cross stands for the mean of the Gaussian fitted distribution; the dotted box will be the second search area obtained from the estimated distribution. An apodised sinc interpolation method used.

C. Registration results

For the buildings with EMS damage grade 0 and 3, the standard deviation (SD) of the registration error is lower than 1 pixel for the test-case of Bam. It is between 1 and 2 pixel for the intact building for test-case of Ryongchon. For the Boumerdes and Muzzafarabad test-cases, the SD of the registration error for grade 0 and 3 is higher; if most of the buildings are precisely registered, some exhibits large errors due to radiometric *natural* changes. The more the damage, the less precise is the registration. The buildings with a collapse of a soft storey in Boumerdes are shown to be difficult to register, because although their roofs are intact, their position and orientation are often unexpected. Finally, another difficulty is pointed out: the imprecision of the SRTM is more sensitive in an area with steep relief (Muzzafarabad), leading to geometric deformations uncorrected by the orthorectification (building deformation, location errors).

IV. DAMAGE ASSESSMENT

The roof of the buildings being registered, one can compare the roofs and thus assess the damage on them between the two dates of acquisition. The correlation coefficient that corresponds to the best offset for each building yields information about the amount of similarity. We use this coefficient to classify the buildings among the different detectable damage classes. We have chosen a supervised classification for the following reasons: we consider that we have no *a priori* knowledge about the number and the different degree of damage classes that are present for a given disaster; moreover, for a given damage degree, the damage feature (here the correlation coefficient) can differ from one test-case to another, according to the type of buildings, to the atmospheric conditions, to the acquisition parameters, etc. However, the required training set is constrained to be small, with five examples per damage

grade. In our case, these examples are randomly selected among the reference database. Finally, because the classification result depends more or less on the chosen training patterns, 100 classification tests are conducted for each case with different training sets, to ensure the robustness of the results.

A. Damage assessment as a function of the test-case

First we investigate the quality of the damage assessment as a regard to the test-case. The rate of buildings that are well classified is computed respectively for every test-case over the whole corresponding reference database, without taking into account the damage degree. Moreover we only consider in this section the pair of QuickBird images so as to compare fairly the results.

For the test-case of Bam, the mean classification performance is 75%, the best performance being 78%. For the Boumerdes test-case, the performance is 70%, with a maximum equal to 72%. For the Muzzafarabad test-case, only 36% of the buildings are well classified, with a maximum performance equal to 39%. Finally, the buildings of the database of the Ryongchon test-case are classified with an mean accuracy of 78% and a maximum performance of 79%.

First, we note the stability of the results as a function of the selected training examples: the mean and the maximum classification performance differ only of 2 to 3 points. It shows that even if the size of the training set is small, the classification method is robust.

We note that the performance are notably lower for the test-case of Muzzafarabad. The damage assessment in this case is unsatisfying. We investigated more precisely this case and noticed important geometric deformations on the buildings between the reference and the crisis images. This is due mainly due to the steep relief that is ineffectively corrected during the orthorectification with the SRTM; the resolution of the DTM is too low. By consequence, the pixel-based similarity measurement used for the registration and for the damage assessment is less efficient. For the other test-cases, the results are quite close and seem satisfactory.

B. Damage assessment as a function of the sensor

The different images pair that have been investigated per test-case are reported in table II. For the test-case of Bam, the classification performances are equal to 75% for the QB/QB case, to 72% for the QB_{1m}/QB_{1m} case and to 67% for the QB/IK case. In this case, the better the resolution, the better the classification performance. We also see that, for the same spatial resolution, the mono-sensor case gives better results than the multisensor case.

For the test-case of Boumerdes, the original QuickBird pair also given better results (70% of buildings correctly classified) than the downsampled ones (64% of buildings correctly classified).

For the test-case of Ryongchon, the difference of performance between the QB/QB pair and the downsampled one is lower (from 78% to 76%). It could be due to the type of damage

that is considered for this case of explosion: damage are either highly visible, or undetectable on the images, whatever the resolution considered.

Finally, for the test-case of Muzzafarabad, the classification performance is equal to 36% for the QB/QB case; regarding this low performance, the downsampled case has not been tested. The IK/IK case gives a result of 32% of buildings well classified. Thus, even if the performances are low, the trend of decrease of performance along with the resolution is confirmed.

C. Damage assessment as a function of the visually estimated damage degree

In this section, the performance of classification is evaluated per damage grade, and the global performance is computed giving the same weight to each class (instead of giving the same weight to each building independently of its damage grade). Because, for each test-case, every damage class has not the same number of buildings than the others, we first note that the global performances differ when evaluating the classification accuracy per damage class. Moreover, classes corresponding to EMS grade 0 and 5 contain more buildings than the intermediate grades. The classification results per class are reported in table III.

For Bam and boumerdes test-cases, the buildings with damage grade 0 and 5 are the most accurately classified. The damage grade 4 is detected with a notably best accuracy than the damage grade 3. Indeed, in the case of Bam, grade 3 corresponds to slight damage on the roof, that do not impact strongly the correlation comparing to the *natural changes* (shadows for example) that appends on most of the intact roofs. In the case of Boumerdes, grade 3 corresponds to buildings with no visible damage on their roof, and with rubbles/dust at their base; hence they are not detected with our method.

For the test-case of Ryongchon, the intact and totally destroyed buildings are detected with the best accuracy. The intermediate class presents more confusion with the other damage classes. For the Bam, Boumerdes and Ryongchon test-cases, the classification results per class are stable; conclusion can be drawn without a loss of generality. Conversely, for the Muzzafarabad test-case, there is an important confusion between the different damage classes. The correlation coefficients are low, whatever the grade considered. The trend is to classify the buildings alternatively between only two classes, the two others being almost ignored. One example of result is shown in table III.

V. Conclusion

We propose in this paper a method to assess damage on buildings in an urban area using a pair of very high resolution images. Its performances are evaluated on several cases, for four different disasters and using images from two sensors. We use as a reference the European macroseismic Scale, and decide to distinguish 4 different damage grades for the buildings in the images.

First, a solution to the problem of registration of building roofs is presented. A method that takes into account the

TABLE III

CLASSIFICATION PERFORMANCES PER DAMAGE GRADE USING THE PAIRS OF ORIGINAL QUICKBIRD IMAGES.

	Events			
	Bam	Boumerdes	Muzzafarabad	Ryongchon
EMS grade 0 / intact	81%	79%	22%	82%
EMS grade 3	20%	0%	52%	
EMS grade 4	68%	31%	4%	
EMS grade 5	91%	91%	87%	
Partially damaged				45%
Totally destroyed				86%

conditions of the image acquisition is proposed. It is based on correlation. The less the damage on the buildings, the better the registration. The roof registration is particularly efficient for the buildings of EMS damage grade 0 and 3.

This preliminary important step of registration being accomplished, we show how the correlation coefficient can be an appropriate feature to efficiently and rapidly classify the buildings in several damage grades using SVM along with a small training set. For three of the four test-cases, the classification performances are between 70% and 80%. The last test-case show the limitations of the method for damage assessment. The reasons of the difficulties encountered are investigated, and we propose some possible solutions.

One could improve the damage assessment if some of the natural changes between the images could be managed. This is notably the case of the shadows created by some elements on the top of the roof, of pixels with specular reflexion and of the geometric deformations uncorrected by the image preprocessing.

These results shows that having a database of the footprint of the buildings before a disaster can lead to an accurate and reliable damage assessment with very high resolution images. GIS of cities tend to be built more and more in order to achieve for example better urban development and environmental management. Such damage assessment using available GIS has yet to be tested.

ACKNOWLEDGMENT

REFERENCES

[1] H. Yésou, Personnal communication, 2005.
[2] G. Grünthal, R. Musson, J. Schwarz, and M. Stucchi, *L'Echelle Macrosismique Europenne 1998.* Cahiers du Centre Europen de Godynamique et de Sismologie, Luxembourg, 2001, vol. 19.
[3] F. Yamazaki, K. Kouchi, M. Matsuoka, M. Kohiyama, and N. Muraoka, "Damage detection from high-resolution satellite images for the 2003 boumerdes, algeria earthquake," in *13th World Conference on Earthquake Engineering, International Association for Earthquake Engineering, Vancouver, British Columbia, Canada,* 2004, p. 13.
[4] F. Yamazaki, Y. Yano, and M. Matsuoka, "Visual damage interpretation of buildings in bam city using quickbird images following the 2003 bam, iran, earthquake," *Earthquake Spectra,* vol. 21, no. S1, pp. S329–S336, December 2005.
[5] B. Adams, C. Huyck, B. Mansouri, R. Eguchi, and M. Shinozuka, "Application of high-resolution optical satellite imagery for post-earthquake damage assessment: The 2003 boumerdes (algeria) and bam (iran) earthquakes," *Research Progress and Accomplishments 2003-2004, Buffalo: MCEER,* 2004, http://mceer.buffalo.edu/publications/resaccom/04-SP01/12_Eguchi.pdf.

[6] G. Bitelli, R. Camassi, L. Gusella, and A. Mongnol, "Image change detection on urban area: the earthquake case," in *XXth ISPRS Congress, Istanbul, Turkey*, July 2004, p. 692.

[7] Z. Chen and T. C. Hutchinson, "Urban damage estimation using statistical processing of satellite images: 2003 bam, iran earthquake," *Proceedings SPIE*, vol. 5667, pp. 289–300, 2005.

[8] M. Sakamoto, Y. Takasago, K. Uto, S. Kakumoto, Y. Kosugi, and T. Doihara, "Automatic detection of damaged area of iran earthquake by high-resolution satellite imagery," in *IEEE Proceedings of International Geoscience and Remote Sensing Symposium 2004*, vol. 2, September 2004, pp. 1418–1421.

[9] K. Kouchi and F. Yamazaki, "Damage detection based on object-based segmentation and classification from high-resolution satellite images for the 2003 boumerdes, algeria earthquake," in *Proceedings of the 26th Asian conference on Remote Sensing, Hanoi, Vietnam*, November 2005.

[10] S. Girard, P. Guerin, H. Maître, and M. Roux, "Building detection from high-resolution color images," *Proceedings of SPIE International Society for Optical Engineering, Image and Signal Processing for Remote Sensing IV Symposium, Barcelona, Spain*, vol. 3500, pp. 278–289, December 1998.

[11] D. Haverkamp, "Automatic building extraction from ikonos imagery," in *Proceedings of the ASPRS 2004, Annual Conference*, May 2004.

[12] T. Kim and J.-P. A. Muller, "Toward an automated building detection system from satellite data," in *Proceedings of SPIE International Society for Optical Engineering, Image and Signal Processing for Remote Sensing II*, vol. 2579, November 1995, pp. 394–404.

[13] A. Shackelford, C. Davis, and W. Xiangyun, "Automated 2-d building footprint extraction from high-resolution satellite multispectral imagery," in *IEEE Proceedings of International Geoscience and Remote Sensing Symposium 2004*, vol. 3, 2004, pp. 1996–1999.

[14] X. Jin and C. Davis, "Automated building extraction from high-resolution satellite imagery in urban areas using structural, contextual, and spectral information," *EURASIP Journal on Applied Signal Processing*, vol. 14, pp. 2196–2206, 2005.

[15] G. Meinel and M. Neubert, "A comparison of segmentation programs for high-resolution remote sensing data," in *Proceedings of the ISPRS 2004 annual conference, Istanbul, Turkey*, July 2004, pp. 1097–1102.

[16] DigitalGlobe. Quickbird specifications. [Online]. Available: http://www.digitalglobe.com/about/quickbird.html

[17] SpaceImaging. Ikonos specifications. [Online]. Available: http://www.spaceimaging.com/products/ikonos/index.htm

[18] U. Thönnessen, G. Hofele, and W. Middelmann, "Change detection in satellite images," in *Proceedings of SPIE Signal Processing, Sensor Fusion, and Target Recognition XIV*, vol. 5809, 2005, pp. 197–207.

[19] J. Canny, "A computational approach to edge detection," *IEEE Transactions on Pattern Analysis and Machine Intelligence*, vol. 8, pp. 679–698, 1986.